



## Original article

# Exploration of the dihydropyrimidine scaffold for the development of new potential anti-inflammatory agents blocking prostaglandin E<sub>2</sub> synthase-1 enzyme (mPGES-1)



Gianluigi Lauro<sup>a</sup>, Maria Strocchia<sup>a</sup>, Stefania Terracciano<sup>a</sup>, Ines Bruno<sup>a,\*</sup>, Katrin Fischer<sup>b</sup>, Carlo Pergola<sup>b</sup>, Oliver Werz<sup>b</sup>, Raffaele Riccio<sup>a</sup>, Giuseppe Bifulco<sup>a,\*</sup>

<sup>a</sup> Department of Pharmacy, University of Salerno, via Giovanni Paolo II, 132, 84084 Fisciano, Italy

<sup>b</sup> Department of Pharmaceutical/Medicinal Chemistry, Institute of Pharmacy, Friedrich Schiller University, Jena, Philosophenweg 14, D-07743 Jena, Germany

## ARTICLE INFO

## Article history:

Received 10 February 2014

Received in revised form

18 April 2014

Accepted 22 April 2014

Available online 24 April 2014

## Keywords:

Molecular docking

Inflammation

mPGES-1 inhibitors

Biginelli reaction

## ABSTRACT

Agents targeting microsomal prostaglandin E<sub>2</sub> synthase-1 (mPGES-1) would inhibit only PGE<sub>2</sub> production induced by inflammatory stimuli and thus could represent a valuable alternative to non-steroidal anti-inflammatory drugs (NSAIDs) as they should be free from the severe side effects of the classic anti-inflammatory drugs. Although several mPGES-1 inhibitors have been so far identified, none of them is currently in clinical trials, therefore the discovery of new molecular platforms, able to interfere with this interesting target, is urgently required. Here, we report the results of a focused collection of dihydropyrimidin-2(1H)-one based molecules projected by Virtual Screening computational techniques. The key interactions with the receptor counterpart were introduced as a qualitative filter for the selection of the most promising compounds. The biological data obtained are consistent with the computer-aided suggestions and disclosed two interesting molecules showing *in vitro* mPGES-1 inhibitory activity in the low μM range.

© 2014 Elsevier Masson SAS. All rights reserved.

## 1. Introduction

Arachidonic acid (AA) is the substrate of several enzymes involved in inflammation events. A first processing of AA by both the constitutively expressed cyclooxygenase (COX)-1 and the inducible COX-2 leads to the production of prostaglandin PGH<sub>2</sub> [1]. PGH<sub>2</sub> is a key intermediate that is downstream transformed into a wide range of inflammatory mediators, including PGE<sub>2</sub>, which possess powerful pleiotropic functions and are mediators of several pathological processes, including chronic inflammation and cancer. In particular, the correlation between increased levels of PGE<sub>2</sub> and the outbreak of arthritis was highlighted in the past few years, and the inhibition of PGE<sub>2</sub> production and signaling is associated with reduction of pain and inflammation [2]. Moreover, an overproduction of PGE<sub>2</sub> is also related to different types of cancer,

including breast, cervical, colorectal, oral, prostate cancers, and multiple myeloma [3].

There are three terminal synthases responsible for PGE<sub>2</sub> biosynthesis: one cytosolic isoform cPGES, and two membrane associated enzymes, mPGES-1 [4] and mPGES-2. cPGES and mPGES-2 are constitutively expressed, while mPGES-1 is an inducible isoform, and in fact its expression is dramatically increased in response of a pro-inflammatory stimulus.

mPGES-1 is a member of Membrane-Associated Proteins in Eicosanoid and Glutathione metabolism (MAPEG) superfamily and is functionally coupled with COX-2. The therapeutic interventions in inflammation so far developed include either the inhibition of COX-1 and COX-2 enzymes by non-steroidal anti-inflammatory drugs (NSAIDs), or selective COX-2 inhibition by coxibs. Nevertheless, they both possess severe gastrointestinal and cardiovascular side-effects that limit their use in long-term treatments as required in chronic inflammation processes [5], prompting to explore new enzymatic targets in this pathway. In this perspective, selective inhibition of mPGES-1 activity has emerged as an alternative promising strategy to develop effective and safer agents helpful in inflammation and in cancer chemoprevention [6]. From a structural point of view, this enzyme shares 39% sequence identity with

**Abbreviations:** GSH, glutathione; MAPEG, membrane-associated proteins in eicosanoid and glutathione metabolism; MGST-1, microsomal glutathione transferase 1; mPGES-1, microsomal prostaglandin E<sub>2</sub> synthase-1; COX, cyclooxygenase; PG, prostaglandin; ADME, absorption, distribution, metabolism, and excretion.

\* Corresponding authors.

E-mail addresses: [brunoin@unisa.it](mailto:brunoin@unisa.it) (I. Bruno), [bifulco@unisa.it](mailto:bifulco@unisa.it) (G. Bifulco).

another MAPEG protein, namely microsomal glutathione transferase-1 (MGST-1). Other related proteins with a less sequence identity are MGST-2, MGST-3, leukotriene C4 (LTC4) synthase, and 5-lipoxygenase-activating protein (FLAP) [7]. In 2008, Jegerschöld et al. presented a 3D-electron crystallography structure of mPGES-1, but the detailed analysis of the protein organization suggested a closed non-active form [8]. In 2013, Sjögren et al. introduced the first high resolution X-ray structure of mPGES-1 in the active form [9], prompting new insights for the structure-based design of new potent inhibitors. The structural details revealed that the protein is a membrane homotrimer with three active sites partially occupied by the cofactor (glutathione, GSH), and recent experimental evidences suggested a 1:3 site reactivity [10]. The asymmetric monomer is characterized by four-helix, and each active site is oriented toward the cytoplasmic part of the protein, in particular between N-terminal parts of helix II and IV of a monomer and the C-terminal part of helix I and the cytoplasmic domain of the adjacent monomer (Fig. 1). This protein folding generates a pronounced deep active site occupied by GSH, and in the outer part, an extended groove between helix I of a monomer and helix IV of the adjacent monomer is observable. mPGES-1 was also co-crystallized with a bis-phenyl GSH-derivative (1-(4-phenylphenyl)-2-(S-glutathionyl)-ethanone). Crystallographic data clearly highlighted the partial replacement of GSH by its derivative; this last showed to keep the same orientation of GSH in the deep cavity of the active site, and a perfect accommodation of the bis-phenyl additional group in the external groove is observed [9].

In recent years, our research group has been deeply involved in the discovery of potential mPGES-1 inhibitors, as promising anti-inflammatory and/or anticancer drugs [11–17]. Based on the additional structural information, we decided to undertake a structure-based drug design with the aim of identifying new molecular platforms able to interfere with the target in object. For our purpose, we decided to rely on dihydropyrimidine nucleus that represents a sort of “privileged structure”, being endowed with several relevant pharmacological effects, including calcium channel modulation for the treatment of cardiovascular diseases,  $\alpha_{1a}$ -adrenergic receptor antagonism, useful for benign prostatic hyperplasia and mitotic kinesin inhibition with anticancer application [18]. In addition to its interesting biological profile, the dihydropyrimidine

core has received a considerable attention in drug-discovery process due to its synthetic accessibility through the easy, cheap and rapid Biginelli one-pot multicomponent reaction [18].

Following this synthetic strategy, a wide number of differently decorated dihydropyrimidin-2(1H)-one-based compounds can be rapidly synthesized combining three synthons: an aldehyde, a 1,3-dicarbonyl compound and an urea. As first step, we performed a focused *in silico* virtual screening on a small set of compounds synthetically accessible by means of molecular docking (1–36, Table 1). A qualitative computational filter, based on the respect of some key interactions with the receptor counterpart, has been introduced, leading to the identification of a focused set of compounds for the subsequent step of chemical synthesis and biological evaluation.

## 2. Results and discussion

### 2.1. Docking studies

Molecular docking calculations were performed using the recently crystallized structure of mPGES-1 (PDB code: 4AL0) [9]. Sjögren et al. have proposed a catalytic process in which GSH covalently binds PGH<sub>2</sub> that subsequently isomerizes to PGE<sub>2</sub> thanks to several amino acid residues close to GSH [9]. A dynamic process in which PGH<sub>2</sub> reaches the binding site and interacts with GSH and the other residues in the active site can be assumed, and then a hypothetical mPGES-1 inhibitor can act either as a false substrate (PGH<sub>2</sub>) or as a cofactor analog (GSH), or at least it can behave in both ways [19]. In the latter case, it can be imagined a scenario in which the inhibitor, in addition to displacing the substrate from its active site, could also influence the binding mode of GSH inside the enzyme pocket. In order to simulate the partial or total displacement of GSH, molecular docking calculations were then performed removing the cofactor from the active site.

We designed new putative dihydropyrimidin-2(1H)-one-featured inhibitors taking into account the synthetic accessibility of the decorated scaffold. Hence, a first computational study was focused on a small set of compounds derived from the combination of the following chemical synthons:

1. Urea, thiourea, or N-methylurea;
2. Ethyl 3-oxobutanoate or ethyl 4-(4-methoxyphenyl)-2,4-dioxobutanoate as 1,3-dicarbonyl compound;
3. Benzaldehyde.

In this way, we obtained a first generation of structurally diverse molecules (1–6) submitted to docking calculations in order to verify the presence of some key interactions with the receptor counterpart:

- $\pi$ – $\pi$  with Tyr130(A), indicative of a good accommodation within the GSH binding site;
- a polar interaction with Ser127(A), a key residue involved in PGH<sub>2</sub> recognition;
- polar interactions with Thr131(A), Gln134(A), and van der Waals interactions with Tyr28(B) and Ile32(B), belonging to the external binding groove.

We noticed that none of these six compounds was able to occupy the external groove, establishing at the same time the  $\pi$ – $\pi$  with Tyr130(A). In particular, compounds 1–3, featuring aliphatic substituents in 5 and 6 positions, were found not able to interact with both the sites, showing only a partial placement in the GSH binding site. However, we found a pose of 4 in which the 4-phenyl group is partially accommodated in the external groove, while the

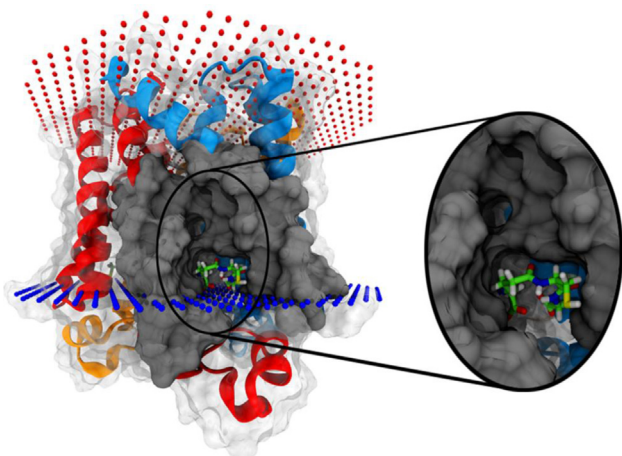
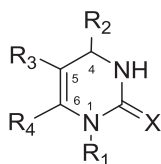


**Fig. 1.** mPGES-1 structure (secondary structure: chain A blue, chain B red, chain C orange); dummy atoms define extracellular (above red atoms) and cytoplasmic (below blue atoms) sides. Glutathione cofactor is depicted in licorice mode (C: green, O red, N, blue, H light gray), molecular surface focused to the GSH binding site and the external binding groove is colored in dark gray. (For interpretation of the references to color in this figure legend, the reader is referred to the web version of this article.)

**Table 1**  
3,4-dihydropyrimidin-2-one derivatives **1–36**.



Entry	R <sub>1</sub>	R <sub>2</sub>	R <sub>3</sub>	R <sub>4</sub>	X
<b>1</b>	H	Phenyl	CO <sub>2</sub> C <sub>2</sub> H <sub>5</sub>	CH <sub>3</sub>	O
<b>2</b>	CH <sub>3</sub>	Phenyl	CO <sub>2</sub> C <sub>2</sub> H <sub>5</sub>	CH <sub>3</sub>	O
<b>3</b>	H	Phenyl	CO <sub>2</sub> C <sub>2</sub> H <sub>5</sub>	CH <sub>3</sub>	S
<b>4</b>	H	Phenyl	4-(methoxybenzoyl)	CO <sub>2</sub> C <sub>2</sub> H <sub>5</sub>	O
<b>5</b>	CH <sub>3</sub>	Phenyl	4-(methoxybenzoyl)	CO <sub>2</sub> C <sub>2</sub> H <sub>5</sub>	O
<b>6</b>	H	Phenyl	4-(methoxybenzoyl)	CO <sub>2</sub> C <sub>2</sub> H <sub>5</sub>	S
<b>7</b>	H	3-Formylphenyl	CO <sub>2</sub> C <sub>2</sub> H <sub>5</sub>	CH <sub>3</sub>	O
<b>8</b>	CH <sub>3</sub>	3-Formylphenyl	CO <sub>2</sub> C <sub>2</sub> H <sub>5</sub>	CH <sub>3</sub>	O
<b>9</b>	H	3-Formylphenyl	CO <sub>2</sub> C <sub>2</sub> H <sub>5</sub>	CH <sub>3</sub>	S
<b>10</b>	H	3-Formylphenyl	4-(methoxybenzoyl)	CO <sub>2</sub> C <sub>2</sub> H <sub>5</sub>	O
<b>11</b>	CH <sub>3</sub>	3-Formylphenyl	4-(methoxybenzoyl)	CO <sub>2</sub> C <sub>2</sub> H <sub>5</sub>	O
<b>12</b>	H	3-Formylphenyl	4-(methoxybenzoyl)	CO <sub>2</sub> C <sub>2</sub> H <sub>5</sub>	S
<b>13</b>	H	3-Ethoxybenzoyl	CO <sub>2</sub> C <sub>2</sub> H <sub>5</sub>	CH <sub>3</sub>	O
<b>14</b>	CH <sub>3</sub>	3-Ethoxybenzoyl	CO <sub>2</sub> C <sub>2</sub> H <sub>5</sub>	CH <sub>3</sub>	O
<b>15</b>	H	3-Ethoxybenzoyl	CO <sub>2</sub> C <sub>2</sub> H <sub>5</sub>	CH <sub>3</sub>	S
<b>16</b>	H	3-Ethoxybenzoyl	4-(methoxybenzoyl)	CO <sub>2</sub> C <sub>2</sub> H <sub>5</sub>	O
<b>17</b>	CH <sub>3</sub>	3-Ethoxybenzoyl	4-(methoxybenzoyl)	CO <sub>2</sub> C <sub>2</sub> H <sub>5</sub>	O
<b>18</b>	H	3-Ethoxybenzoyl	4-(methoxybenzoyl)	CO <sub>2</sub> C <sub>2</sub> H <sub>5</sub>	S
<b>19</b>	H	(4-cyanophenyl)pyridin-2-yl	CO <sub>2</sub> C <sub>2</sub> H <sub>5</sub>	CH <sub>3</sub>	O
<b>20</b>	CH <sub>3</sub>	(4-cyanophenyl)pyridin-2-yl	CO <sub>2</sub> C <sub>2</sub> H <sub>5</sub>	CH <sub>3</sub>	O
<b>21</b>	H	(4-cyanophenyl)pyridin-2-yl	CO <sub>2</sub> C <sub>2</sub> H <sub>5</sub>	CH <sub>3</sub>	S
<b>22</b>	H	(4-cyanophenyl)pyridin-2-yl	4-(methoxybenzoyl)	CO <sub>2</sub> C <sub>2</sub> H <sub>5</sub>	O
<b>23</b>	CH <sub>3</sub>	(4-cyanophenyl)pyridin-2-yl	4-(methoxybenzoyl)	CO <sub>2</sub> C <sub>2</sub> H <sub>5</sub>	O
<b>24</b>	H	(4-cyanophenyl)pyridin-2-yl	4-(methoxybenzoyl)	CO <sub>2</sub> C <sub>2</sub> H <sub>5</sub>	S
<b>25</b>	H	6,8-Dibromo-4-oxo-4H-chromen-3-yl	CO <sub>2</sub> C <sub>2</sub> H <sub>5</sub>	CH <sub>3</sub>	O
<b>26</b>	CH <sub>3</sub>	6,8-Dibromo-4-oxo-4H-chromen-3-yl	CO <sub>2</sub> C <sub>2</sub> H <sub>5</sub>	CH <sub>3</sub>	O
<b>27</b>	H	6,8-Dibromo-4-oxo-4H-chromen-3-yl	CO <sub>2</sub> C <sub>2</sub> H <sub>5</sub>	CH <sub>3</sub>	S
<b>28</b>	H	6,8-Dibromo-4-oxo-4H-chromen-3-yl	4-(methoxybenzoyl)	CO <sub>2</sub> C <sub>2</sub> H <sub>5</sub>	O
<b>29</b>	CH <sub>3</sub>	6,8-Dibromo-4-oxo-4H-chromen-3-yl	4-(methoxybenzoyl)	CO <sub>2</sub> C <sub>2</sub> H <sub>5</sub>	O
<b>30</b>	H	6,8-Dibromo-4-oxo-4H-chromen-3-yl	4-(methoxybenzoyl)	CO <sub>2</sub> C <sub>2</sub> H <sub>5</sub>	S
<b>31</b>	H	5-(3-(trifluoromethyl)phenyl)furan-2-yl	CO <sub>2</sub> C <sub>2</sub> H <sub>5</sub>	CH <sub>3</sub>	O
<b>32</b>	CH <sub>3</sub>	5-(3-(trifluoromethyl)phenyl)furan-2-yl	CO <sub>2</sub> C <sub>2</sub> H <sub>5</sub>	CH <sub>3</sub>	O
<b>33</b>	H	5-(3-(trifluoromethyl)phenyl)furan-2-yl	CO <sub>2</sub> C <sub>2</sub> H <sub>5</sub>	CH <sub>3</sub>	S
<b>34</b>	H	5-(3-(trifluoromethyl)phenyl)furan-2-yl	4(methoxybenzoyl)	CO <sub>2</sub> C <sub>2</sub> H <sub>5</sub>	O
<b>35</b>	CH <sub>3</sub>	5-(3-(trifluoromethyl)phenyl)furan-2-yl	4(methoxybenzoyl)	CO <sub>2</sub> C <sub>2</sub> H <sub>5</sub>	O
<b>36</b>	H	5-(3-(trifluoromethyl)phenyl)furan-2-yl	4(methoxybenzoyl)	CO <sub>2</sub> C <sub>2</sub> H <sub>5</sub>	S

5-(4-methoxybenzoyl) moiety is properly oriented to establish a  $\pi$ - $\pi$  with Tyr130(A) (Fig. 2). A similar binding mode was found for 1-(N-methyl) derivative **5** and for the thio-analog **6**.

Since the remaining part of the external groove was not occupied by the meta-position of the 4-phenyl group, we decided to gradually expand the substitutions in this direction. Preserving all the other substituents, a new set of compounds featuring a new 4-(3-formyl-phenyl) moiety was evaluated (**7–12**). In addition, while a better accommodation of 5-(4-methoxybenzoyl) group was found, the external groove was still not fully occupied (pose related to **10** in Fig. S1, Supporting Information).

Also in this case, compounds **7–9**, featuring aliphatic substituents in C5 and C6, were not found compatible with this binding mode. For these reasons, we decided to progressively increase the steric hindrance at the C4 position of the dihydropyrimidine scaffold, with the introduction of 3-ethoxybenzyl (**13–18**), (4-cyanophenyl)pyridine-2-yl (**19–24**), (6,8 dibromo-4-oxo-4H-chromen-3-yl) (**25–30**), and 5-(3-(trifluoromethyl)phenyl)furan-2-yl (**31–36**) substituents, respectively. The selection of heteroaromatic rings derived from the aim of increasing the possible polar interaction with the hydrophilic residues in the external groove. Also in these cases, docking poses satisfying the contemporary  $\pi$ - $\pi$  interaction with Tyr130(A) were found only in compounds

featuring 5-(3-methoxybenzoyl) and 6-ethylcarboxylate groups. Docking calculations showed for 4-(3-ethoxybenzyl) derivatives a binding mode comparable to that found for the previously considered 4-(3-formylphenyl) derivatives (pose related to **16**, Fig. S2, Supporting Information).

Furthermore, together with the  $\pi$ - $\pi$  interaction between the 4-methoxybenzoyl in C5 and Tyr130 (A), only a partial accommodation of the larger 4-cyanophenyl (pyridine-2-yl) and 6,8 dibromo-4-oxo-4H-chromen-3-yl substituents in the external groove was detected (poses related to **22** and **28**, Figs S3 and S4, Supporting Information, respectively). Regarding compounds **34–36**, docking analysis showed that the orientation of the 4-(5-(3-(trifluoromethyl)phenyl)furan-2-yl) moiety allows better interactions with the binding groove counterpart (Fig. 3).

## 2.2. Chemistry and biological assays

In order to corroborate our computational results, we firstly decided to synthesize compounds **10**, **16**, **22**, **28**, **34** and to submit them to biological screening. In particular, as in docking simulations we observed a similar behavior for urea, thiourea and N-methylurea derivatives, we utilized only urea as Biginelli reaction synthon. With the optimized general conditions reported in

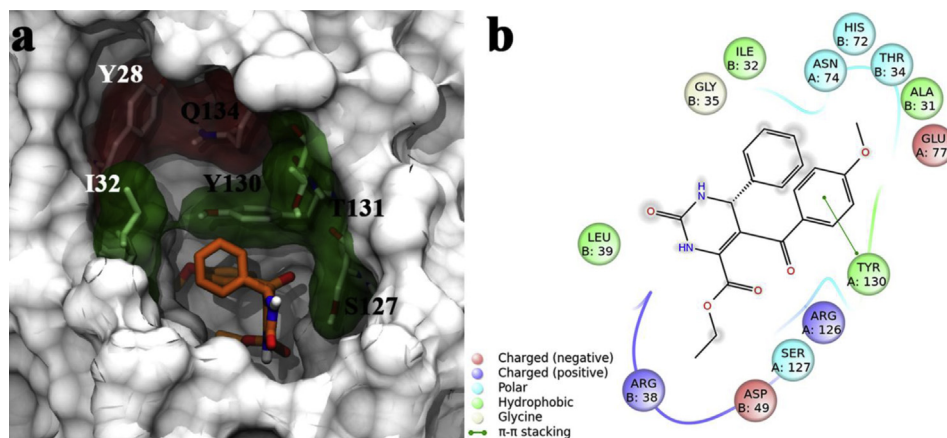


**Fig. 2.** a) 3D model of **4** (colored by atom types: C orange, N blue, O red, H light gray) in docking with mPGES-1 (molecular surface represented in white); residues in the active site represented in licorice (colored by atom types: C white, N blue, O red, H light gray; black captions for residues in chain A and white captions for those in chain B) and related molecular surfaces depicted in transparent green (for residues able to interact with **4**) and transparent red (for residues not able to interact with **4**). b) 2D panel representing interactions between **4** and residues in mPGES-1 binding site. (For interpretation of the references to color in this figure legend, the reader is referred to the web version of this article.)

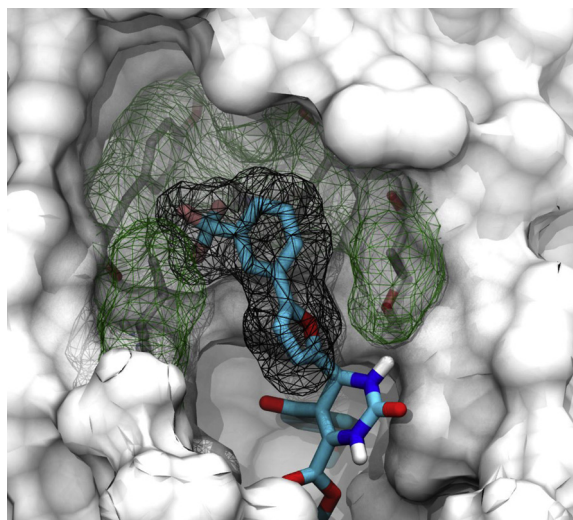


**Fig. 3.** Shape complementarity between 6-(5-(3-(trifluoromethyl)phenyl)furan-2-yl) substituent (molecular surface represented in black wireframes) and external binding groove of mPGES-1 (molecular surface of residues in this site represented in green wireframes). (For interpretation of the references to color in this figure legend, the reader is referred to the web version of this article.)

**Scheme 1**, the synthesis of these compounds was performed through a microwave-assisted Biginelli reaction, which provides a rapid access to substituted dihydropyrimidine derivatives with good yields and in a short reaction time [20]. Urea or its derivatives (1.5 equiv), two different 1,3-dicarbonyl compounds (1.0 equiv) and the appropriate aryl/heteroaryl aldehydes (1.0 equiv), were successfully used in a high-speed trimethylsilyl chloride (TMSCl)-mediated Biginelli condensation, using microwave irradiation. Synthesized compounds were then purified by reversed-phase HPLC and characterized by ESI-MS, HRMS and NMR spectra (see Experimental Section).

Interference of the test compounds with mPGES-1 activity was investigated in a cell-free assay using the microsomal fraction of interleukin-1 $\beta$ -stimulated human A549 cells [21]. Inhibition of mPGES-1 by our compounds was perfectly in line with computational predictions. In fact, among the tested compounds, an interesting  $IC_{50}$  value of  $4.16 \pm 0.47 \mu\text{M}$  was detected for compound **34**,

confirming our suggestions regarding the appropriate accommodation of a putative inhibitor in the mPGES-1 binding site.

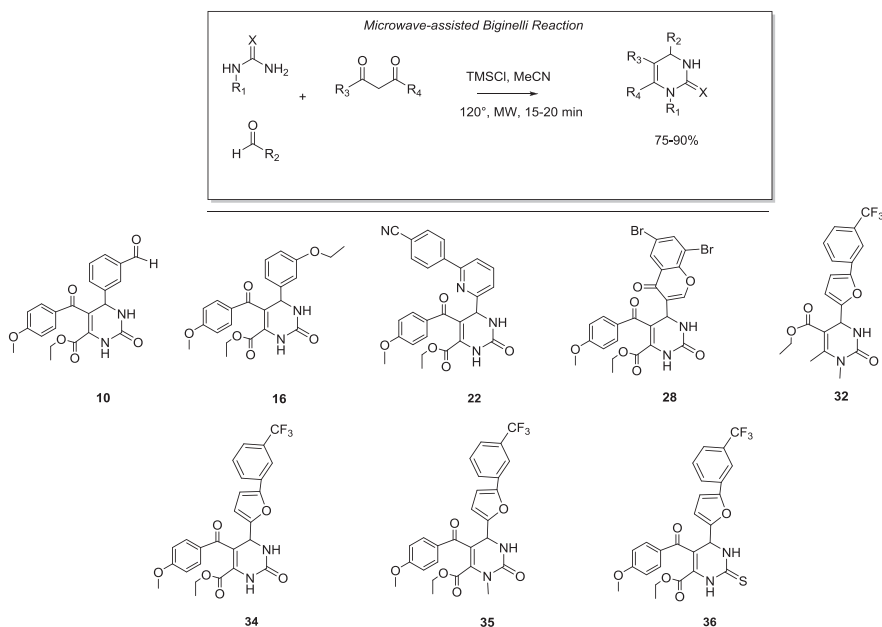
Moreover, maintaining the crucial 4-, 5- and 6- substituents on the dihydropyrimidine core, we synthesized and tested the biological activity of the two **34**-related compounds, namely the N1-methyl derivative **35** and the thio-analog **36**. The results obtained showed efficient inhibitory activity for **35** ( $IC_{50} = 7.56 \pm 0.94 \mu\text{M}$ ), but a weak and incomplete suppression of mPGES-1 activity for **36** (37% inhibition at  $10 \mu\text{M}$ ,  $IC_{50} > 30 \mu\text{M}$ ) (Fig. 4 and Table 2). Since the docking model of **36** confirms the respect of the key interactions found for **34** and **35** (Fig. S5, Supporting Information), the differences in biological activities could be mainly ascribed to the influence of the chemical properties of sulfur vs. oxygen (such as dimensions, electronegativity), not properly weighted by the scoring functions of the docking software.

To further confirm that the presence of both 4-methoxybenzoyl group at C5, and 5-(3-(trifluoromethyl)phenyl)furan-2-yl group at C4 is necessary for the activity, compound **32** was synthesized as negative control. As expected, compound **32**, lacking the aromatic substituent at C5 was found inactive. This confirms our hypothesis of using a proper qualitative structure-based filter to subsequently integrate with the docking predicted binding affinities (Table S1, Supporting Information) for the selection of new mPGES-1 inhibitors. In Fig. 5 the docking model related to the active compound **34** is depicted. The 5-(3-methoxybenzoyl) group establishes a  $\pi$ - $\pi$  interaction with Tyr130(A), while the bulky 4-(5-(3-(trifluoromethyl)phenyl)furan-2-yl) substituent occupies the external binding groove, interacting with Thr31(B), Ile32(B), Gln134(A), and Leu135(A); more specifically, trifluoromethyl terminal group contributes to these interactions, making contacts with Tyr28(B). The 6-ethylcarboxylate function interacts with a shallow groove directed toward the cytoplasmic side of the protein, while the urea containing portions of the molecules establish polar contacts with Ser127(A). Similar binding modes have been observed for the derivatives **35** and **36** (Fig. 6, and S5), while **32** lacked these fundamental interactions.

### 3. Materials and methods

#### 3.1. Computational details

The chemical structures of investigated compounds were built with Maestro (version 9.6) [22] Build Panel and then processed with LigPrep, version 2.8 [22], generating all the possible



**Scheme 1.** General synthetic procedure and chemical structures of synthesized dihydropyrimidine derivatives.

stereoisomers, tautomers, protonation states at a pH of  $7.4 \pm 1.0$ , and finally minimized using OPLS 2005 force field. For the subsequent docking calculations, all the structures were converted in the .pdbqt format using OpenBabel software (version 2.3.2) [23], adding Gasteiger charges.

Protein 3D model was prepared using the Schrödinger Protein Preparation Wizard [22], starting from the mPGES-1 X-ray structure in the active form (PDB code: 4AL0). In particular, crystallized water molecules and GSH cofactor were removed, all hydrogens were added, and bond orders were assigned. Conformation “A” was chosen for residues crystallized in two conformations, as reported in the original PDB file. Protein .pdb file obtained was then processed with Autodock Tools 1.5.6 and converted in .pdbqt format, merging non polar hydrogens and adding Gasteiger charges. Charge deficit was spread over all atoms of related residues.

Docking calculations were performed using the Autodock-Vina software [24]. In the configuration file linked to 3D structure of the protein, we specified coordinates and dimensions along  $x$ ,  $y$ ,  $z$  axes of the grid related to the site of presumable pharmacological interest. In particular, we chose the binding site between A and B chains, and a grid box size of  $24 \times 20 \times 18$  and centered at 10.304 ( $x$ ),  $-11.033$  ( $y$ ), and  $-8.384$  ( $z$ ) was set, with spacing of 1.0 Å between the grid points. The exhaustiveness value was set to 512, saving 30 conformations as maximum number of binding modes. For all the investigated compounds, all open-chain bonds were treated as active torsional bonds. Docking results were analyzed with Autodock Tools 1.5.6. Illustrations of the 3D models were generated using VMD software [25] and Maestro [22].

### 3.2. Chemistry

All commercially available starting materials were purchased from Sigma–Aldrich and were used as received. All solvents used for the synthesis were of HPLC grade; they were purchased from Sigma–Aldrich and Carlo Erba Reagenti. All NMR spectra ( $^1\text{H}$ , HMBC, HSQC) were recorded on a Bruker Avance 600 MHz instrument at  $T = 298\text{ K}$  ( $^1\text{H}$  at 600 MHz,  $^{13}\text{C}$  at 150 MHz). All compounds were dissolved in 0.5 mL of 99.95%  $\text{CDCl}_3$  (Carlo Erba, 99.95 Atom % D). Coupling constants ( $J$ ) are reported in Hertz, and

chemical shifts are expressed in parts per million (ppm) on the delta ( $\delta$ ) scale relative to  $\text{CHCl}_3$  (7.26 ppm for  $^1\text{H}$  and 77.2 ppm for  $^{13}\text{C}$ ) as internal reference. Electrospray mass spectrometry (ESI-MS) was performed on a LCQ DECA TermoQuest (San José, California, USA) mass spectrometer. High resolution mass spectra were acquired on a LTQ Orbitrap XL (Thermo Scientific). Reactions were monitored on silica gel 60 F<sub>254</sub> plates (Merck) and visualized with cerium sulfate and under UV ( $\lambda = 254\text{ nm}$ , 365 nm). Analytical and semi-preparative reversed-phase HPLC was performed on Agilent Technologies 1200 Series high performance liquid chromatography using a Jupiter Proteo C<sub>18</sub> reversed-phase column ( $250 \times 4.60\text{ mm}$ ,  $4\mu\text{m}$ , 90 Å, flow rate = 1 mL/min;  $250 \times 10.00\text{ mm}$ ,  $10\mu\text{m}$ , 90 Å, flow rate = 4 mL/min respectively, Phenomenex®). The binary solvent system (A/B) was as follows: 0.1% TFA in water (A) and 0.1% TFA in  $\text{CH}_3\text{CN}$  (B). The absorbance was detected at 280 nm. The purity of all tested compound (>98%) was determined by HPLC analysis.

#### 3.2.1. Microwave irradiation experiments

All microwave irradiation experiments were carried out in a dedicated CEM-Discover® Focused Microwave Synthesis apparatus, operating with continuous irradiation power from 0 to 300 W utilizing the standard absorbance level of 300 W maximum power. The reactions were carried out in 10 mL sealed microwave glass vials. The Discover™ system also offers controllable ramp time, hold time (reaction time) and uniform stirring. The temperature was monitored using the CEM-Discover built-in-vertically-focused IR temperature sensor. After the irradiation period, the reaction vessel was cooled rapidly (60–120 s) to ambient temperature by air jet cooling.

#### 3.2.2. General procedure for microwave-assisted Biginelli reaction

A mixture of appropriate aldehyde (1.0 mmol), urea or its derivatives (thiourea and *N*-methylurea) (1.5 mmol), 1,3-dicarbonyl compound (1.0 mmol) in acetonitrile (1.5 mL) were placed in a 10 mL microwave glass vial equipped with a small magnetic stirring bar. TMSCl (1.0 mmol) was added and the mixture was then stirred under microwave irradiation at 120 °C for 15–20 min. After irradiation, the reaction mixture was cooled to ambient temperature by air jet cooling, cold water was added and the vial was poured

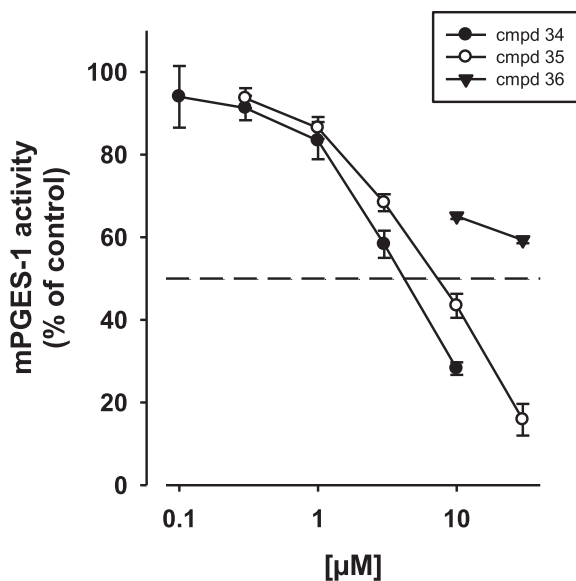


**Fig. 4.** Concentration-response analysis of compounds **34**, **35**, and **36** for inhibition of mPGES-1 in a cell-free assay. Data are given as mean  $\pm$  SEM,  $n = 3$ .

**Table 2**  
mPGES-1 inhibition by tested compounds **10**, **16**, **22**, **28**, **32**, **34**, **35**, **36**.

Compound ID	IC <sub>50</sub> + SEM ( $\mu$ M) <sup>a</sup>
<b>10</b>	n.a.
<b>16</b>	n.a.
<b>22</b>	n.a.
<b>28</b>	n.a.
<b>32</b>	n.a.
<b>34</b>	4.16 $\pm$ 0.47
<b>35</b>	7.56 $\pm$ 0.94
<b>36</b>	>30

<sup>a</sup> n.a.: no activities at concentration lower than 10  $\mu$ M found.

into crushed ice and then at 4 °C overnight. The resulting precipitate was filtered and washed with a cold mixture of ethanol/water (1:1) (3  $\times$  3 mL), to give the desired product in good yields (75–90%). HPLC purification was performed by semi-preparative

reversed-phase HPLC (on a Jupiter Proteo C<sub>18</sub> column: 250  $\times$  10.00 mm, 10  $\mu$ , 90 Å, flow rate = 4 mL/min) using the gradient conditions reported below for each compound. The final products were obtained with high purity > 98% detected by HPLC analysis and were fully characterized by ESI-MS, HRMS and NMR spectra.

**3.2.2.1. Compound 10.** Compound **10** was obtained by following the general procedure as a yellow gelatinous solid (120.9 mg, 85% yield). RP-HPLC  $t_R = 24.7$  min, gradient condition: from 5% B to 25% B in 10 min, increased to 100% B in 45 min, flow rate of 4 mL/min,  $\lambda = 280$  nm. <sup>1</sup>H NMR (500 MHz, CDCl<sub>3</sub>):  $\delta = 0.85$  (t,  $J = 7.1$  Hz, 3H), 3.81 (s, 3H), 3.88–4.01 (m, 4H), 5.59 (s, 1H), 6.77 (d,  $J = 8.9$  Hz, 2H), 7.44 (t,  $J = 7.8$  Hz, 1H), 7.53–7.61 (m, 3H), 7.76 (br s, 2H), 9.92 (s, 1H); <sup>13</sup>C NMR (125 MHz, CDCl<sub>3</sub>):  $\delta = 13.7, 54.6, 57.8, 61.9, 112.7, 113.3, 128.4, 128.8, 130.7, 131.6, 132.0, 133.2, 190.7$ . ESMS, calcd for C<sub>22</sub>H<sub>20</sub>N<sub>2</sub>O<sub>6</sub> 408.13; found  $m/z = 409.1$  [M + H]<sup>+</sup>. HRMS, calcd for C<sub>22</sub>H<sub>21</sub>N<sub>2</sub>O<sub>6</sub> [M + H]<sup>+</sup> 409.1400, found 409.1388.

**3.2.2.2. Compound 16.** Compound **16** was obtained by following the general procedure as a brown gelatinous solid (132.5 mg, 78% yield). RP-HPLC  $t_R = 22.9$  min, gradient condition: from 5% B to 30% B in 10 min, increased to 100% B in 40 min, flow rate of 4 mL/min,  $\lambda = 280$  nm. <sup>1</sup>H NMR (500 MHz, CDCl<sub>3</sub>):  $\delta = 0.85$  (t,  $J = 7.1$  Hz, 3H), 1.33 (t,  $J = 7.1$  Hz, 3H), 3.79 (s, 3H), 3.85–3.98 (m, 4H), 5.46 (s, 1H), 6.72–6.82 (m, 4H), 7.13 (t,  $J = 7.8$  Hz, 1H), 7.35 (br s, 1H), 7.57 (d,  $J = 8.8$  Hz, 2H); <sup>13</sup>C NMR (125 MHz, CDCl<sub>3</sub>):  $\delta = 13.2, 14.2, 56.1, 55.9, 56.1, 59.6, 113.4, 113.9, 114.2, 119.6, 119.8, 130.7, 131.4, 131.7$ . ESMS, calcd for C<sub>23</sub>H<sub>24</sub>N<sub>2</sub>O<sub>6</sub> 424.16; found  $m/z = 425.2$  [M + H]<sup>+</sup>. HRMS calcd for C<sub>23</sub>H<sub>25</sub>N<sub>2</sub>O<sub>6</sub> [M + H]<sup>+</sup> 425.1713, found 425.1692.

**3.2.2.3. Compound 22.** Compound **22** was obtained by following the general procedure as a yellow powder (144 mg, 79%); RP-HPLC  $t_R = 20.8$  min, gradient condition: from 20% B to 100% B in 45 min, flow rate of 4 mL/min,  $\lambda = 280$  nm. <sup>1</sup>H NMR (500 MHz, CDCl<sub>3</sub>):  $\delta = 0.83$  (t,  $J = 7.1$  Hz, 3H), 3.74 (s, 3H), 3.84–3.99 (m, 2H), 5.62 (s, 1H), 6.71 (d,  $J = 9.0$  Hz, 2H), 7.24–7.37 (m, 1H), 7.60–7.63 (m, 4H), 7.74–7.88 (m, 4H); <sup>13</sup>C NMR (125 MHz, CDCl<sub>3</sub>):  $\delta = 13.4, 55.6, 59.7, 62.9, 113.5, 114.0, 120.1, 120.3, 127.3, 127.7, 129.8, 131.4, 141.4$ . ESMS, calcd for C<sub>27</sub>H<sub>22</sub>N<sub>4</sub>O<sub>5</sub> 482.16; found  $m/z = 483.1$  [M + H]<sup>+</sup>. HRMS calcd for C<sub>27</sub>H<sub>23</sub>N<sub>4</sub>O<sub>5</sub> [M + H]<sup>+</sup> 483.1668, found 483.1636.

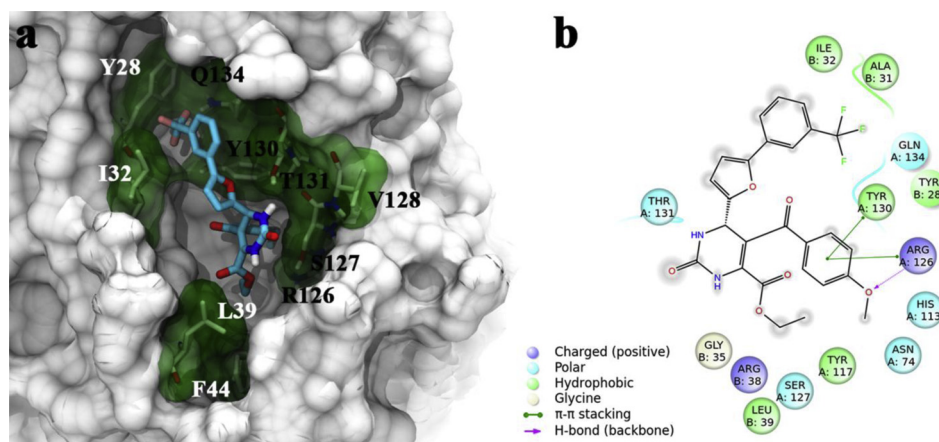


**Fig. 5.** a) 3D model of identified inhibitor **34** (colored by atom types: C sky blue, N blue, O red, H light gray, F pink) in docking with mPGES-1 (molecular surface represented in white); residues in the active site represented in licorice (colored by atom types: C white, N blue, O red, H light gray); black captions for residues in chain A and white captions for those in chain B) and related molecular surfaces depicted in transparent green. b) 2D panel representing interactions between **34** and residues in mPGES-1 binding site (the legend related to the 2D panel is reported in the lower part of the figure). (For interpretation of the references to color in this figure legend, the reader is referred to the web version of this article.)

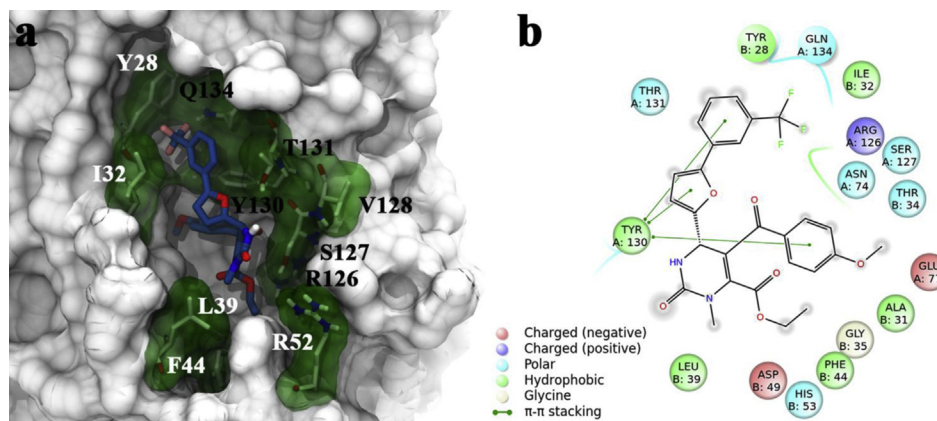


**Fig. 6.** a) 3D model of compound **35** (colored by atom types: C blue, N blue, O red, H light gray) in docking with mPGES-1 (molecular surface represented in white); residues in the active site represented in licorice (colored by atom types: C white, N blue, O red, H light gray); black captions for residues in chain A and white captions for those in chain B) and related molecular surfaces depicted in transparent green. b) 2D panel representing interactions between **35** and residues in mPGES-1 binding site. (For interpretation of the references to color in this figure legend, the reader is referred to the web version of this article.)

**3.2.2.4. Compound 28.** Compound **28** was obtained by following the general procedure as a yellow powder (68.7 mg, 75% yield); RP-HPLC  $t_R = 26.4$  min, gradient condition: from 5% B to 30% B in 5 min, increased to 100% B in 45 min, flow rate of 4 mL/min,  $\lambda = 280$  nm.  $^1\text{H}$  NMR (500 MHz,  $\text{CDCl}_3$ ):  $\delta = 0.98$  (t,  $J = 7.1$  Hz, 3H), 3.88 (s, 3H), 4.02–4.12 (m, 2H), 5.42 (s, 1H), 6.98 (d,  $J = 8.7$  Hz, 2H), 7.10 (s, 1H), 7.92 (d,  $J = 8.7$  Hz, 2H), 8.03 (br s, 1H), 8.25 (br s, 1H);  $^{13}\text{C}$  NMR (125 MHz,  $\text{CDCl}_3$ ):  $\delta = 13.0, 61.7, 62.7, 75.3, 112.5, 127.4, 130.7, 135.3, 136.3, 148.5, 157.4$ . ESMS, calcd for  $\text{C}_{24}\text{H}_{18}\text{Br}_2\text{N}_2\text{O}_7$  606.22; found  $m/z = 606.8$   $[\text{M} + \text{H}]^+$ . HRMS, calcd for  $\text{C}_{24}\text{H}_{19}\text{Br}_2\text{N}_2\text{O}_7$   $[\text{M} + \text{H}]^+$  604.9559, found 604.9533.

**3.2.2.5. Compound 32.** Compound **32** was obtained by following the general procedure as a red solid (67.3 mg, 75% yield); RP-HPLC  $t_R = 26.7$  min, gradient condition: from 5% B to 40% B in 10 min, increased to 100% B in 40 min, flow rate of 4 mL/min,  $\lambda = 280$  nm.  $^1\text{H}$  NMR (500 MHz,  $\text{CDCl}_3$ ):  $\delta = 1.29$  (t,  $J = 7.1$  Hz, 3H), 2.55 (s, 3H), 3.26 (s, 3H), 4.10–4.20 (m, 2H), 5.52 (s, 1H), 6.21 (d,  $J = 3.3$  Hz, 1H), 6.62 (d,  $J = 3.3$  Hz, 1H), 7.45–7.52 (m, 3H), 7.81 (br s, 1H);  $^{13}\text{C}$  NMR (125 MHz,  $\text{CDCl}_3$ ):  $\delta = 13.7, 14.8, 32.6, 56.0, 60.2, 108.0, 110.8, 127.4, 128.6, 130.3, 133.5$ . ESMS, calcd for  $\text{C}_{20}\text{H}_{19}\text{F}_3\text{N}_2\text{O}_4$  408.13; found  $m/z = 409.1$   $[\text{M} + \text{H}]^+$ . HRMS, calcd for  $\text{C}_{20}\text{H}_{20}\text{F}_3\text{N}_2\text{O}_4$   $[\text{M} + \text{H}]^+$  409.1375, found 409.1354.

**3.2.2.6. Compound 34.** Compound **34** was obtained by following the general procedure as a red gelatinous solid (149.2 mg, 88% yield); RP-HPLC  $t_R = 34.2$  min, gradient condition: from 5% B to 35% B in 15 min, increased to 100% B in 40 min, flow rate of 4 mL/min,  $\lambda = 280$  nm.  $^1\text{H}$  NMR (500 MHz,  $\text{CDCl}_3$ ):  $\delta = 0.85$  (t,  $J = 7.1$  Hz, 3H), 3.74 (s, 3H), 3.85–4.00 (m, 2H), 5.59 (s, 1H), 6.37 (d,  $J = 3.3$  Hz, 1H), 6.57 (d,  $J = 3.3$  Hz, 1H), 6.75 (d,  $J = 8.4$  Hz, 2H), 7.41–7.47 (m, 2H), 7.60 (br s, 2H), 7.73 (d,  $J = 8.4$  Hz, 2H);  $^{13}\text{C}$  NMR (125 MHz,  $\text{CDCl}_3$ ):  $\delta = 13.7, 52.7, 55.4, 63.0, 107.5, 109.7, 111.6, 116.8, 121.7, 124.4, 127.0, 129.5, 130.8, 131.7$ . ESMS, calcd for  $\text{C}_{26}\text{H}_{21}\text{F}_3\text{N}_2\text{O}_6$  514.14; found  $m/z = 515.1$   $[\text{M} + \text{H}]^+$ . HRMS, calcd for  $\text{C}_{26}\text{H}_{22}\text{F}_3\text{N}_2\text{O}_6$   $[\text{M} + \text{H}]^+$  515.1430, found 515.1403.

**3.2.2.7. Compound 35.** Compound **35** was obtained by following the general procedure as a red gelatinous solid (84.3 mg, 76% yield); RP-HPLC  $t_R = 30.3$  min, gradient condition: from 5% B to 40% B in 10 min, increased to 100% B in 40 min, flow rate of 4 mL/min,  $\lambda = 280$  nm.  $^1\text{H}$  NMR (500 MHz,  $\text{CDCl}_3$ ):  $\delta = 1.05$  (t,  $J = 7.1$  Hz, 3H), 3.20 (s, 3H), 3.82 (s, 3H), 3.76–3.88 (m, 2H), 5.54 (s, 1H), 6.40 (d,  $J = 3.3$  Hz, 1H), 6.60 (d,  $J = 3.3$  Hz, 1H), 6.87 (d,  $J = 8.7$  Hz, 2H), 7.48

(br s, 2H), 7.66–7.73 (m, 4H);  $^{13}\text{C}$  NMR (125 MHz,  $\text{CDCl}_3$ ):  $\delta = 13.7, 32.6, 50.8, 56.0, 63.5, 108.0, 110.8, 114.6, 120.7, 121.2, 121.7, 127.4, 128.6, 130.3, 133.5$ . ESMS, calcd for  $\text{C}_{27}\text{H}_{24}\text{F}_3\text{N}_2\text{O}_6$  528.15; found  $m/z = 529.1$   $[\text{M} + \text{H}]^+$ . HRMS, calcd for  $\text{C}_{27}\text{H}_{24}\text{F}_3\text{N}_2\text{O}_6$  529.1586, found 529.1564.

**3.2.2.8. Compound 36.** Compound **36** was obtained by following the general procedure as a pale brown solid (122.7 mg, 90% yield); RP-HPLC  $t_R = 32.3$  min, gradient condition: from 5% B to 35% B in 10 min, increased to 100% B in 40 min, flow rate of 4 mL/min,  $\lambda = 280$  nm.  $^1\text{H}$  NMR (500 MHz,  $\text{CDCl}_3$ ):  $\delta = 0.85$  (t,  $J = 7.1$  Hz, 3H), 3.75 (s, 3H), 3.85–4.00 (m, 2H), 5.58 (s, 1H), 6.42 (d,  $J = 3.3$  Hz, 1H), 6.58 (d,  $J = 3.3$  Hz, 1H), 6.78 (d,  $J = 8.7$  Hz, 2H), 7.43–7.51 (m, 2H), 7.60 (br s, 2H), 7.74 (d,  $J = 8.7$  Hz, 2H);  $^{13}\text{C}$  NMR (125 MHz,  $\text{CDCl}_3$ ):  $\delta = 13.7, 52.2, 55.1, 62.8, 107.4, 110.7, 113.6, 113.8, 120.4, 124.0, 126.8, 128.9, 129.2, 131.1$ . ESMS, calcd for  $\text{C}_{26}\text{H}_{21}\text{F}_3\text{N}_2\text{O}_5\text{S}$  530.11; found  $m/z = 531.1$   $[\text{M} + \text{H}]^+$ . HRMS, calcd for  $\text{C}_{26}\text{H}_{22}\text{F}_3\text{N}_2\text{O}_5\text{S}$   $[\text{M} + \text{H}]^+$  531.1202, found 531.1172.

### 3.3. Bioactivity assays

#### 3.3.1. Assay systems and materials

Dulbecco's Modified Eagle Medium (DMEM)/high glucose (4.5 g/L) medium, penicillin, streptomycin, trypsin/ethylenediaminetetraacetate (EDTA) solution, and LSM 1077 lymphocyte separation medium were obtained from PAA (Pasching, Austria). IL-1 $\beta$  was obtained from ReproTech (Hamburg, Germany). Fetal calf serum (FCS), phenylmethylsulfonyl fluoride (PMSF), leupeptin, soybean trypsin inhibitor (STI), glutathione (reduced), PGB<sub>1</sub>, lysozyme,  $\text{Ca}^{2+}$ -ionophore A23187, and arachidonic acid were obtained from Sigma–Aldrich (Deisenhofen, Germany). MK886 and 11 $\beta$ -PGE<sub>2</sub> were obtained from Cayman Chemical (Ann Arbor, MI). PGE<sub>2</sub>, adenosine triphosphate (ATP), isopropyl- $\beta$ -d-1-thiogalactopyranoside (IPTG), and dextrane were obtained from Larodan (Malmö, Sweden), Roche Diagnostics (Mannheim, Germany), AppliChem (Darmstadt, Germany), and Fluka (Neu-Ulm, Germany), respectively. A549 cells were provided by the Karolinska Institute (Stockholm, Sweden). Leukocyte concentrates from human healthy volunteers were provided by Institute of Transfusion Medicine, University Hospital Jena, Germany.

#### 3.3.2. Cell culture

A549 cells were grown in DMEM/high glucose (4.5 g/mL) medium supplemented with heat-inactivated FCS (10%, v/v), penicillin

(100 U/mL) and streptomycin (100 µg/mL). After three days, confluent cells were detached using  $1 \times$  trypsin/EDTA and reseeded with a density of  $1 \times 10^5$  cells/ml medium.

### 3.3.3. Preparation of crude mPGES-1 in microsomes of A549 cells and determination of mPGE<sub>2</sub> synthase activity

Preparation of A549 cells and determination of mPGES-1 activity was performed as described previously [26]. In brief, A549 cells were treated with 1 ng/mL interleukin-1 $\beta$  for 48 h at 37 °C and 5% CO<sub>2</sub>. After sonification, the homogenate was subjected to differential centrifugation at  $10,000 \times g$  for 10 min and  $174,000 \times g$  for 1 h at 4 °C. The pellet (microsomal fraction) was resuspended in 1 mL homogenization buffer (0.1 M potassium phosphate buffer pH 7.4, 1 mM phenylmethanesulphonyl fluoride, 60 µg/mL soybean trypsin inhibitor, 1 µg/mL leupeptin, 2.5 mM glutathione, and 250 mM sucrose), and the total protein concentration was determined. Microsomal membranes were diluted in potassium phosphate buffer (0.1 M, pH 7.4) containing 2.5 mM glutathione. Test compounds or vehicle were added, and after 15 min at 4 °C, the reaction (100 µL total volume) was initiated by addition of PGH<sub>2</sub> (20 µM, final concentration, unless stated otherwise). After 1 min at 4 °C, the reaction was terminated using stop solution (100 µL; 40 mM FeCl<sub>2</sub>, 80 mM citric acid, and 10 µM of 11 $\beta$ -PGE<sub>2</sub> as internal standard). PGE<sub>2</sub> was separated by solid phase extraction and analyzed by RP-HPLC as described. [26]

### 3.3.4. Statistics

Data are expressed as mean  $\pm$  SE. IC<sub>50</sub> values were graphically calculated from measurements at 4–5 different concentrations of the compounds using SigmaPlot 9.0 (Systat Software Inc., San Jose, USA). The program Graphpad Instat (Graphpad Software Inc., San Diego, CA) was used for statistical comparisons. Statistical evaluation of the data was performed by one-way ANOVAs for independent or correlated samples followed by Tukey HSD post-hoc tests. Where appropriate, Student's *t* test for paired and correlated samples was applied. A *P* value of <0.05 was considered significant.

## 4. Conclusions

In conclusion, we have reported the structure-based design of a focused collection of decorated dihydropyrimidin-2(1H)-ones as new potential mPGES-1 inhibitors. Docking calculations allowed us to identify compounds **34** and **35** able to inhibit mPGES-1 activity with IC<sub>50</sub> in the low micromolar range, and allowed to disclose the dihydropyrimidine scaffold as a new molecular platform useful for the development of new and more potent inhibitors. A careful structure–activity relationship analysis shed more light on the decoration pattern of the scaffold essential for the activity. Furthermore, all the investigated compounds showed a stereocenter at C4 position and here the substituent always adopts the same orientation, as emerged by the analysis of the binding modes. Stereoselective syntheses will be further evaluated in order to assess if privileged enantiomers, at least in theory, show a highest binding affinities for the target enzyme.

## Acknowledgments

Financial support by Associazione Italiana Ricerca sul Cancro (AIRC) Grant IG\_12777 – Bifulco Giuseppe.

## Appendix A. Supplementary data

Supplementary data related to this article can be found at <http://dx.doi.org/10.1016/j.ejmech.2014.04.061>.

## References

- [1] M.E. Turini, R.N. DuBois, Cyclooxygenase-2: a therapeutic target, *Annual Review of Medicine* 53 (2002) 35–57.
- [2] J.M. McCoy, J.R. Wicks, L.P. Audoly, The role of prostaglandin E2 receptors in the pathogenesis of rheumatoid arthritis, *The Journal of Clinical Investigation* 110 (2002) 651–658.
- [3] M. Nakanishi, V. Gokhale, E.J. Meuillet, D.W. Rosenberg, mPGES-1 as a target for cancer suppression, *Biochimie* 92 (2010) 660–664.
- [4] B. Samuelsson, R. Morgenstern, P.J. Jakobsson, Membrane prostaglandin E synthase-1: a novel therapeutic target, *Pharmacological Reviews* 59 (2007) 207–224.
- [5] D. Mukherjee, S.E. Nissen, E.J. Topol, Risk of cardiovascular events associated with selective COX-2 inhibitors, *Journal of the American Medical Association* 286 (2001) 954–959.
- [6] C.E. Trebino, J.L. Stock, C.P. Gibbons, B.M. Naiman, T.S. Watchmann, J.P. Umland, K. Pandher, J.M. Lapointe, S. Saha, M.L. Roach, D. Carter, N.A. Thomas, B.A. Durtschi, J.D. McNeish, J.E. Hambor, P.J. Jakobsson, T.J. Carty, J.R. Perez, L.P. Audoly, Impaired inflammatory and pain responses in mice lacking an inducible prostaglandin E synthase, *Proceedings of the National Academy of Sciences of the United States of America* 100 (2003) 9044–9049.
- [7] P.J. Jakobsson, S. Thoren, R. Morgenstern, B. Samuelsson, Identification of human prostaglandin E synthase: a microsomal, glutathione-dependent, inducible enzyme, constituting a potential novel drug target, *Proceedings of the National Academy of Sciences of the United States of America* 96 (1999) 7220–7225.
- [8] C. Jegerschöld, S. Pawelzik, P. Purhonen, P. Bhakat, K.R. Gheorghe, N. Gyobu, K. Mitsuoka, R. Morgenstern, P. Jakobsson, H. Hebert, Structural basis for induced formation of the inflammatory mediator prostaglandin E2, *Proceedings of the National Academy of Sciences of the United States of America* 105 (2008) 11110–11115.
- [9] T. Sjögren, J. Nord, M. Ek, P. Johansson, G. Liu, S. Geschwindner, Crystal structure of microsomal prostaglandin E2 synthase provides insight into diversity in the MAPEG superfamily, *Proceedings of the National Academy of Sciences of the United States of America* 110 (2013) 3806–3811.
- [10] S. He, Y. Wu, D. Yu, L. Lai, Microsomal prostaglandin E synthase-1 exhibits one-third-of-the-sites reactivity, *The Biochemical Journal* 440 (2011) 13–21.
- [11] M.D. Guerrero, M. Aquino, I. Bruno, M.C. Terencio, M. Paya, R. Riccio, L. Gomez-Paloma, Synthesis and pharmacological evaluation of a selected library of new potential anti-inflammatory agents bearing the gamma-hydroxybutenolide Scaffold: a new class of inhibitors of prostanoid production through the selective modulation of microsomal prostaglandin E synthase-1 expression (mPGES-1), *Journal of Medicinal Chemistry* 50 (2007) 2176–2184.
- [12] M. Aquino, M.D. Guerrero, I. Bruno, M.C. Terencio, M. Paya, R. Riccio, Development of a second generation of inhibitors of microsomal prostaglandin E synthase 1 expression bearing the gamma-hydroxybutenolide scaffold, *Bioorganic & Medicinal Chemistry* 16 (2008) 9056–9064.
- [13] M.D. Guerrero, M. Aquino, I. Bruno, R. Riccio, M.C. Terencio, M. Payá, Anti-inflammatory and analgesic activity of a novel inhibitor of microsomal prostaglandin E synthase-1 expression, *European Journal of Pharmacology* 620 (2009) 112–119.
- [14] R. De Simone, R.M. Andres, M. Aquino, I. Bruno, M.D. Guerrero, M.C. Terencio, M. Paya, R. Riccio, Toward the discovery of new agents able to inhibit the expression of microsomal prostaglandin E synthase-1 enzyme as promising tools in drug development, *Chemical Biology & Drug Design* 76 (2010) 17–24.
- [15] R. De Simone, M.G. Chini, I. Bruno, R. Riccio, D. Mueller, O. Werz, G. Bifulco, Structure-based discovery of inhibitors of microsomal prostaglandin E2 synthase-1, 5-lipoxygenase and 5-lipoxygenase-activating protein: promising hits for the development of new anti-inflammatory agents, *Journal of Medicinal Chemistry* 54 (2011) 1565–1575.
- [16] R. De Simone, I. Bruno, R. Riccio, K. Stadler, J. Bauer, A.M. Schaible, S. Laufer, O. Werz, Identification of new  $\gamma$ -hydroxybutenolides that preferentially inhibit the activity of mPGES-1, *Bioorganic & Medicinal Chemistry* 20 (2012) 5012–5016.
- [17] M.G. Chini, R. De Simone, I. Bruno, R. Riccio, F. Dehm, C. Weinigel, D. Barz, O. Werz, G. Bifulco, Design and synthesis of a second series of triazole-based compounds as potent dual mPGES-1 and 5-lipoxygenase inhibitors, *European Journal of Medicinal Chemistry* 54 (2012) 311–323.
- [18] a) D. Dallinger, C.O. Kappe, Creating chemical diversity space by scaffold decoration of dihydropyrimidines, *Pure and Applied Chemistry* 77 (2005) 155–161;  
b) C.O. Kappe, Biologically active dihydropyrimidones of the Biginelli – type-a literature survey, *European Journal of Medicinal Chemistry* 35 (2000) 1043–1052.
- [19] S. He, L. Lai, Molecular docking and competitive binding study discovered different binding modes of microsomal prostaglandin E synthase-1 inhibitors, *Journal of Chemical Information and Modeling* 51 (2011) 3254–3261.
- [20] a) L. Pisani, H. Prokopcová, J.M. Kremser, C.O. Kappe, 5-Aroyl-3,4-dihydropyrimidin-2-one library generation via automated sequential and parallel microwave-assisted synthesis techniques, *Journal of Combinatorial Chemistry* 9 (2007) 415–421;  
b) A. Stadler, C.O. Kappe, Automated library generation using sequential

- microwave-assisted chemistry. Application toward the Biginelli multicomponent condensation, *Journal of Combinatorial Chemistry* 3 (2001) 624–630.
- [21] A. Koeberle, U. Siemoneit, U. Buehring, H. Northoff, S. Laufer, W. Albrecht, O. Werz, Licofelone suppresses prostaglandin E2 formation by interference with the inducible microsomal prostaglandin E2 synthase-1, *The Journal of Pharmacology and Experimental Therapeutics* 326 (2008) 975–982.
- [22] **Schrodinger, LLC, New York, NY, 2013.**
- [23] N.M. O'Boyle, M. Banck, C.A. James, C. Morley, T. Vandermeersch, G.R. Hutchison, Open Babel: an open chemical toolbox, *Journal of Cheminformatics* 3 (2011) 33.
- [24] O. Trott, A.J. Olson, AutoDock Vina: improving the speed and accuracy of docking with a new scoring function, efficient optimization and multi-threading, *Journal of Computational Chemistry* 31 (2010) 455–461.
- [25] W. Humphrey, A. Dalke, K. Schulten, VMD – visual molecular dynamics, *Journal of Molecular Graphics* 14 (1996) 33–38.
- [26] A. Koeberle, H. Zettl, C. Greiner, M. Wurglics, M. Schubert-Zsilavec, O. Werz, Pirinixic acid derivatives as novel dual inhibitors of microsomal prostaglandin E2 synthase-1 and 5-lipoxygenase, *Journal of Medicinal Chemistry* 51 (2008) 8068–8076.